ELSEVIER

Contents lists available at ScienceDirect

## Dyes and Pigments

journal homepage: www.elsevier.com/locate/dyepig





## A versatile luminescent probe for sensing and monitoring amyloid proteins

Guillem Vázquez <sup>a,c</sup>, Alba Espargaró <sup>b,c</sup>, Ana B. Caballero <sup>a,c,\*</sup>, Ania Di Pede-Mattatelli <sup>b</sup>, M. Antònia Busquets <sup>b,c</sup>, Daria Nawrot <sup>a,1</sup>, Raimon Sabaté <sup>b,c,\*\*</sup>, Ernesto Nicolás <sup>a</sup>, Jordi Juárez-Jiménez <sup>b,d</sup>, Patrick Gamez <sup>a,c,e,\*\*\*</sup>

- <sup>a</sup> Department of Inorganic and Organic Chemistry, Faculty of Chemistry, University of Barcelona, Martí I Franquès 1-11, 08028, Barcelona, Spain
- b Department of Pharmacy and Pharmaceutical Technology and Physical-Chemistry, Faculty of Pharmacy and Food Sciences, University of Barcelona, Avda. Joan XXIII 27-31, 08028, Barcelona, Spain
- <sup>c</sup> Institute of Nanoscience and Nanotechnology (IN2UB), Universitat de Barcelona, 08028, Barcelona, Spain
- <sup>d</sup> Institut of Theoretical and Computational Chemistry (IQTC), University of Barcelona, 08028, Barcelona, Spain
- <sup>e</sup> Catalan Institution for Research and Advanced Studies, Passeig Lluís Companys 23, 08010, Barcelona, Spain

#### ARTICLE INFO

#### Keywords: Fluorescent probe Amyloids Protein identification 1,8-Naphthalimide

#### ABSTRACT

A modified lysine residue containing an environment-sensitive moiety was prepared through a straightforward synthesis, and its fluorescent properties were examined. The new fluorescent sensor, DMN-BocK, can monitor amyloid aggregation processes associated with neurodegenerative diseases such as Alzheimer's or Parkinson's. DMN-BocK offers advantages over classical amyloid-specific dyes like Thioflavins or Congo Red because it is (1) available to detect a broader range of amyloid structures; (2) useful both *in vitro* and *in cellulo*; (3) capable of differentiating amyloid structures, providing information on the binding site microenvironment; and (4) a synthon than can be incorporated into protein sequences to gain further structural information. Our findings suggest that DMN-based amino-acid probes have a strong potential to become a sensor of choice for *in vitro* and *in cellulo* studies of amyloid aggregation in drug discovery assays.

#### 1. Introduction

Fluorescence spectroscopy is one of the most convenient and powerful techniques in biophysics. It is specific, sensitive, non-destructive, easy to use, fast, inexpensive, and allows real-time measurements *in vitro*, *in cellulo* and *in vivo*. Thanks to the increasing diversity and affordability of emissive probes, this technique is being used extensively [1,2].

Solvatochromic fluorophores are sensitive to the pola rity of the local environment. They display high quantum yields in nonpolar solvents or hydrophobic surroundings, and low emission in polar environments [3]. Typically, they are push-pull dyes that undergo intramolecular charge transfer upon light absorption, which creates a highly dipolar excited state. The interaction of the excited state with the dipoles of polar

solvents lowers its energy while destabilizing the ground state. Consequently, the dye emission shifts to longer wavelengths and lower quantum yields because the non-radiative decay increases with solvent polarity [4].

The highly sensitive photophysical behavior of solvatochromic fluorophores makes them particularly suitable for real-time reporting of biological dynamic processes such as protein-protein interactions, conformational changes, self-assembly and aggregation [3,5–9]. Within this class of fluorophores, 4-*N*,*N*-dimethylaminonaphthalimide (4-DMN) derivatives show strong fluorescence when excited at wavelengths over 400 nm, and their quantum yield usually varies with the polarity of the local solvent environment. They have been explored for detecting biomolecular interactions [10,11], subcellular localization of receptors [12], assessing enzyme reactivity [13], evaluating protein

<sup>\*</sup> Corresponding author. Department of Inorganic and Organic Chemistry, Faculty of Chemistry, University of Barcelona, Martí I Franquès 1-11, 08028, Barcelona, Spain

<sup>\*\*</sup> Corresponding author. Department of Pharmacy and Pharmaceutical Technology and Physical-Chemistry, Faculty of Pharmacy and Food Sciences, University of Barcelona, Avda. Joan XXIII 27-31, 08028, Barcelona, Spain.

<sup>\*\*\*</sup> Corresponding author. Department of Inorganic and Organic Chemistry, Faculty of Chemistry, University of Barcelona, Martí i Franquès 1-11, 08028, Barcelona, Spain.

E-mail addresses: ana.caballero@ub.edu (A.B. Caballero), rsabate@ub.edu (R. Sabaté), patrick.gamez@qi.ub.es (P. Gamez).

Present address: Faculty of Pharmacy in Hradec Králové, Charles University, 50005, Hradec Králové, Czech Republic.

G. Vázquez et al.

hydrophobicity [14], targeting lysosomal HSA [15], and generating cell imaging probes [13,16]. However, 4-DMN derivatives have been scarcely used for detecting amyloids [8,17-21]. Amyloids are misfolded proteins in insoluble conformation characterized by the presence of  $\beta$ -sheet-rich fibrils. They are associated with an array of over forty human illnesses, ranging from non-neurological disorders such as type 2 diabetes to neurological diseases such as Alzheimer's and prion diseases. Detection of amyloids has primarily been conducted using aggregation-induced emission (AIE) and twisted intramolecular charge transfer (TICT) chromophores [22]. For instance, TICT-type thioflavins T (ThT) and S (ThS) are the most commonly used fluorescent probes for studying amyloid aggregation [23-25]. AIE and TICT dyes can exhibit strong fluorescence and, potentially, blue-shifted emission when the molecules form or bind to aggregates, resulting from the restriction of intramolecular bond rotation (Chart 1, left) [24-27]. In contrast, the photophysical properties of solvatochromic fluorophores - including maximum excitation and emission wavelengths ( $\lambda_{ex}$  and  $\lambda_{em}$ ), fluorescence quantum yields ( $\Phi_f$ ), and fluorescence lifetimes ( $\tau$ ) – are sensitive to the nature of the local microenvironment [3].

Herein, we report the synthesis and photophysical characterization of a new solvatochromic probe, DMN-BocK, which is a water-soluble tert-butyloxycarbonyl (Boc)-protected natural amino acid (lysine) with an appended 4-DMN moiety (Chart 1). The appended Boc-lysine increases the solubility of the probe in water while allowing it to be incorporated into the primary sequence of a peptide. We found that the photochemical properties of DMN-BocK enable the detection of subtle polarity variations within the binding pockets of a range of proteins which adopt amyloid conformation: Aβ40 and tau (Alzheimer's disease), α-synuclein (Parkinson's disease), non-mammalian prions such as HET-s PFD, Ure2p, and Sup35, mammalian prions such as vPrP from voles, and amylin (type 2 diabetes). Our results illustrate how this molecular sensor surpasses amyloid probes of choice (thioflavins) and provides further information regarding the conformation of amyloid fibrils (polymorphs) while enabling monitoring of the aggregation process both in vitro and in living cells such as bacteria.

#### 2. Experimental Section

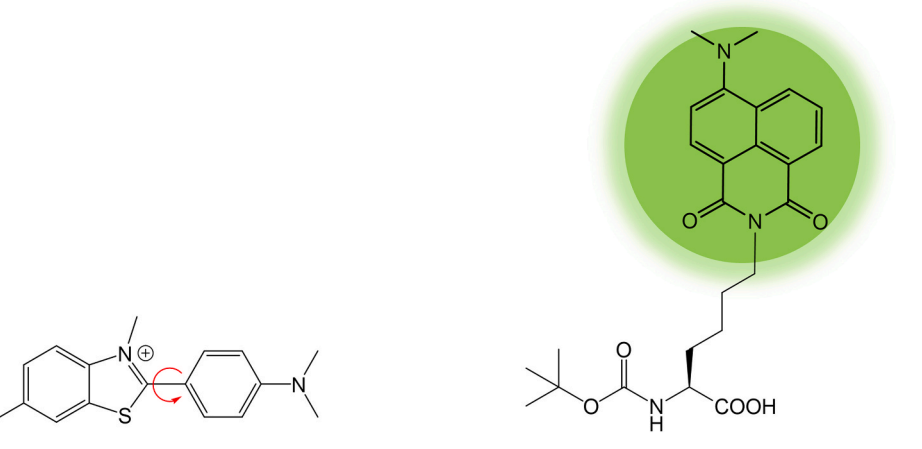
### 2.1. General instrumentation

<sup>1</sup>H NMR spectra were recorded on a 400 MHz Varian Mercury-400 (100.6 MHz for <sup>13</sup>C NMR) spectrometer with proton decoupling. 2D

NMR measurements (COSY, HSQC, and HMBC) were used to fully characterize the compounds. The chemical shifts are reported in ppm relative to residual CHCl<sub>3</sub> as an internal reference for  ${}^{1}$ H ( $\delta$  7.26 ppm) downfield to TMS. For <sup>13</sup>C, the chemical shifts in ppm are referenced to the carbon resonances of CDCl $_3$  ( $\delta$  77.16 ppm). The NMR data were analyzed using MestReNova 9.1.0 and they are reported as follows: s, singlet; d, doublet; t, triplet; q, quartet; m, multiplet; app, apparent. Coupling constants are given in Hz. High-resolution electrospray ionization mass spectrometry (HR ESI-MS) was performed using an LC/ MSD-TOF spectrometer with an Agilent 1100 HPLC pumping system in either positive or negative-ion modes. HR ESI-MS spectra were processed with MassHunter Workstation Software. Qualitative Analysis Version B.02.00 Build 2.0.197.7 (Agilent Technologies). Both instruments are located at the Centres Científics i Tecnològics of the Universitat de Barcelona (CCiTUB). IR spectra of the solid products were obtained using a Thermo Scientific Nicolet 6700 FT-IR spectrophotometer equipped with an attenuated total reflectance (ATR) accessory. UV-Vis spectra were recorded with a Varian Cary 100 spectrophotometer at room temperature; 1 cm path length quartz cuvettes were used. The hydrodynamic diameter of the aggregates formed by DMN-BocK in different solvents, and at 50 µM concentration, was determined by dynamic light scattering at a fixed scattering angle of 90° with a Zetasizer Nano (Malvern, UK) at 25 °C. For TEM, carbon-coated copper grids of 200 mesh were activated through glow discharge for 30 s, before casting the protein samples followed by a thorough washing with ultrapure water. The grids were treated with UranyLess (EMS) and left to dry in a desiccator for at least 24 h. The samples were visualized at the Centres Científics i Tecnològics of the Universitat de Barcelona (CCiTUB), using a Tecnai Spirit TWIN (FEI) 120 kV TEM microscope equipped with a LaB6 emitter and a Megaview  $1k \times 1k$  CCD. Partition coefficients of ThT and DMN-Boc were calculated using PerkinElmer ChemOffice 2020 software package.

## 2.2. Preparation of DMN-BocK

4-N,N-Dimethylamino-1,8-naphthalic anhydride. A solution of 4-bromo-1,8-naphthalic anhydride (2.72 g, 9.8 mmol) in 3-methyl-1-butanol (55 mL) was refluxed and 3-dimethylamino-propionitrile (4.44 mL, 39.3 mmol) was subsequently added. The initial white suspension progressively turned into an orange solution, which was refluxed overnight. The orange solid formed upon cooling at room temperature was filtered out and washed with cold water and cold



Thioflavin T (ThT)

DMN-BocK

Chart 1. Representation of the molecular structures of ThT (TICT fluorophore and probe of choice for amyloids), and of the newly-described DMN-BocK (solvatochromic fluorophore).

isohexane to afford 1.69 g (71 %) of the final product.

Orange solid. R<sub>f</sub> (AcOEt with 0.5 % AcOH): 0.75. <sup>1</sup>H NMR (CDCl<sub>3</sub>, 400 MHz):  $\delta$  3.11 (s, 6H, H<sub>11</sub>), 7.08 (d, 1H, J = 8.4 Hz, H<sub>3</sub>), 7.65 (dd, 1H, J = 7.3 Hz, J = 8.5 Hz, H<sub>6</sub>), 8.39 (d, 1H, J = 8.3 Hz, H<sub>2</sub>), 8.46 (dd, 1H, J = 1.1 Hz, J = 8.5 Hz, H<sub>5</sub>), 8.52 (dd, 1H, J = 1.1 Hz, J = 7.3 Hz, H<sub>7</sub>) ppm. <sup>13</sup>C NMR (CDCl<sub>3</sub>, 100.6 MHz):  $\delta$  44.6 (C<sub>11</sub>), 109.2 (C<sub>1</sub>), 113.1 (C<sub>3</sub>), 119.1 (C<sub>8</sub>), 124.7 (C<sub>4a</sub>), 124.9 (C<sub>6</sub>), 132.8 (C<sub>5</sub> + C<sub>8a</sub>), 133.1 (C<sub>7</sub>), 134.9 (C<sub>2</sub>), 157.8 (C<sub>4</sub>), 160.6 (C<sub>10</sub>), 161.6 (C<sub>9</sub>) ppm. IR (cm<sup>-1</sup>): 747, 774, 996, 1014, 1339, 1566, 1584, 1717. See atom numbering in Scheme 1 and full spectra in Figures A.1-A.4.

 $N\alpha$ -Boc- $N\varepsilon$ -(4-N,N-dimethylamino-1,8-naphthalimido)-L-lysine (DMN-BocK). The synthesis of DMN-BocK was carried out as previously reported for the alanine analogue [10]. Briefly, a three-necked round-bottomed flask containing 4-N,N-dimethylamino-1,8-naphthalic anhydride (1.59 g, 6.6 mmol) and equipped with a magnetic stirrer, a reflux condenser and a dropping funnel was purged with N2. Then, 1, 4-dioxane (150 mL) was transferred into the flask and the resulting brown suspension was refluxed under stirring. An aqueous solution (30 mL) of Boc-Lysine-OH (1.49 g, 6.0 mmol) and NaHCO<sub>3</sub> (2.52 g, 30.0 mmol) was added dropwise, and the resulting yellow mixture was stirred for 2.5 h. The vellow suspension was allowed to cool to room temperature and the solvent was evaporated under reduced pressure. The crude product was diluted with deionized water (150 mL) and acidified with 4 M HCl to pH 6-7 in the presence of DCM (50 mL). The aqueous phase was extracted with DCM, dried over anhydrous MgSO<sub>4</sub>, and evaporated under reduced pressure. The resulting bright orange solid (1.71 g, 60 %) was used without further purification.

Orange solid.  $R_f$  (AcOEt with 0.5 % AcOH): 0.55. MS (HR ESI+): m/z calculated for  $[C_{25}H_{31}N_3O_6 + H]^+$  470.2286, found 470.2282.  $^1H$  NMR (CDCl $_3$ , 400 MHz):  $\delta$  1.41 (s, 9H,  $H_{13}$ ), 1.45–1.55 (m, 2H,  $H_{\gamma}$ ), 1.68–1.79 (m, 2H,  $H_{\delta}$ ), 1.80–1.99 (m, 2H,  $H_{\beta}$ ), 3.07 (s, 6H,  $H_{11}$ ), 4.08–4.20 (m, 2H,  $H_{\epsilon}$ ), 4.23–4.31 (m, 1H,  $H_{\alpha}$ ), 7.06 (d, 1H, J = 8.2,  $H_{3}$ ), 7.62 ( $t_{app}$ , 1H,  $J_{app}$  = 8.0 Hz,  $H_{\delta}$ ), 8.38 (d, 1H, J = 8.4,  $H_{5}$ ), 8.43 (d, 1H, J = 8.2,  $H_{2}$ ), 8.52 (d, 1H, J = 7.2 Hz,  $H_{7}$ ) ppm.  $^{13}$ C NMR (CDCl $_{3}$ , 100.6 MHz):  $\delta$  22.7 ( $C_{\gamma}$ ), 27.6 ( $C_{\delta}$ ), 28.3 (C13), 31.6 ( $C_{\beta}$ ), 39.48 ( $C_{\epsilon}$ ), 44.7 (C11), 53.5 ( $C_{\alpha}$ ), 79.9 (C12), 113.3 (C3), 114.7 (C1), 122.9 (C8), 124.8 (C6), 125.1 (C4a), 130.2 (C8a), 131.1 (C7), 131.2 (C5), 132.8 (C2), 155.9 (C14), 157.0 (C4), 164.2 (C10), 164.7 (C9), 176.5 (C15) ppm. IR (cm $^{-1}$ ): 752, 792, 1161, 1361, 1570, 1637, 1682, 2856, 2928. See atom numbering in Scheme 1 and full spectra in Figures A.5-A.8.

## 2.3. Fluorescence spectroscopy and determination of relative quantum yield values

All fluorescence measurements were made at room temperature using a HORIBA Jobin–Yvon iHR320 spectrofluorometer. The instrument excitation and emission slits were both set at 5 nm. The spectra were collected with 200  $\mu L$  quartz cuvettes of 1 cm optical path length. The measurements were carried out with ThT ( $\lambda_{ex}=445$  nm) and DMN-BocK ( $\lambda_{ex}=420$  nm).

The relative fluorescence quantum-yield values of DMN-BocK in different solvents were calculated at the excitation wavelength of 440 nm using Eq. (1):

$$\Phi = \Phi_R \frac{I}{I_R} \frac{OD_R}{OD} \frac{n^2}{n_o^2} \tag{1}$$

where  $\Phi$  and  $\Phi_R$  are the respective fluorescence quantum yield of the dye and the reference, I and  $I_R$  are the respective integrated fluorescence spectra of the dye and the reference, OD and  $OD_R$  are the respective absorption at the excitation wavelength (440 nm) of the dye and the reference, and n and  $n_R$  are the respective refractive indexes of the solvent. Fluorescein in 0.01 M NaOH was used as a reference dye ( $\Phi_R = 0.91$ ). The  $\Phi$  values were collected over the 470–700 nm emission band.

Time-correlated single photon counting (TCSPC) were performed on an Edinburgh Instruments FS-5 spectrophotometer equipped with a SC-25 thermostated sample holder set to 20  $^{\circ}$ C unless specified otherwise, and the samples excited at 446.2 nm using an EPL-450 ps pulsed diode laser.

The Lippert-Mataga analysis was carried out by using Eq. (2):

$$\overline{\nu}_{ss} = \left[ \frac{2(\mu_e - \mu_g)^2}{hca^3} \right] \Delta f + \overline{\nu}_{ss}^o \tag{2}$$

where  $\bar{\nu}_{ss}$  is the Stokes shift, the superscript "°" indicates the absence of solvent,  $\mu_g$  and  $\mu_g$  are dipole moments in the ground state and the excited state, respectively, and a is Onsager cavity radius. The orientation polarizability  $\Delta f$  is defined as Eq. (3)

$$\Delta f = \left[\frac{\varepsilon - 1}{2\varepsilon + 1}\right] - \left[\frac{n^2 - 1}{2n^2 + 1}\right] \tag{3}$$

where  $\varepsilon$  and n are the solvent dielectric constant and its refractive index,

**DMN-BocK (60 %)** 

Scheme 1. Two-step synthesis of DMN-BocK, and atom numbering used for NMR assignment.

respectively.

# 2.4. Monitoring of in vitro $A\beta 40$ aggregation kinetics by light scattering, ThT fluorescence, and DMN-BocK fluorescence

A FLUOstar Omega plate reader (BMG Labtech) was used in absorbance mode for scattering (360 nm) and fluorescence mode (top optics) with filters of ex440/em490, and ex440/em530 for reading ThT and DMN-BocK fluorescence, respectively. Solid Aβ40 aliquots (see preparation in Supp. Info) were dissolved in 30  $\mu$ L DMSO and sonicated for 15 min. In 96-well plates, the samples were brought to 200  $\mu$ L with 100 mM HEPES pH 7.4, yielding final concentrations of 10  $\mu$ M Aβ40, 10  $\mu$ M ThT (for ThT samples), 10  $\mu$ M DMN-BocK (for DMN-BocK samples) and 3 % DMSO. Stock solutions of 2 mM ThT and 2 mM DMN-BocK in DMSO were used. Endpoint measurements were performed immediately after sample preparation at 37 °C every 5 min, 700 rpm.

# 2.5. $A\beta40$ aggregation kinetics monitored by ThS and DMN-BocK fluorescence in bacterial cells

Escherichia coli competent cells BL21 (DE3) were transformed with the pET28a vector from Novagen (Merck-Millipore, USA) carrying the DNA sequence of Aβ40. A CLARIOstar plate reader (BMG Labtech) in top optics configuration was used in fluorescence mode with the filters ex445/em485 and ex440/em530 for ThS and DMN-BocK, respectively. Optical density at 600 nm was determined in a DTX 800 multimode reader (Beckman Coulter) to normalize the fluorescence based on the bacterial concentration. Bacteria samples were brought to the plate (100 μL) in triplicate. Endpoint measurements were initiated immediately after IPTG addition, at 37 °C every 5 min, 700 rpm.

#### 2.6. Fluorescence microscopy in bacteria

Bacterial cells overexpressing A $\beta$ 42, A $\beta$ 40, and tau (see also Appendix 1), respectively, were incubated for 1 h with 20  $\mu$ M DMN-BocK. The excess of DMN-BocK was removed by centrifugation and the cells were resuspended in PBS and placed on a microscope slide. Images were obtained under LED light using a CYR70010 filter or using phase contrast in a Leica Thunder microscope equipped with an sCMOS camera (Leica K5) at the Centres Científics i Tecnològics of the Universitat de Barcelona (CCiTUB).

## 2.7. Molecular docking

The binding of DMN-BocK and ThT to A $\beta$ 40 fibrils was investigated using docking calculations performed with rDock [28] employing the 20 conformers (obtained from solid-state NMR) with PDBid reference 2M4J [29] as target structures. To accommodate the voluminous DMN probe in the NMR models, each structure of the A $\beta$ 40 trimer was replicated on each face of the fibril, leading to docking structures consisting of nine A $\beta$ 40 monomers. Each protein model was then prepared with Maestro, and protonation states were assigned at pH 7.4 using PROPKA [30]. A protein-wide docking strategy was followed defining a docking box of 64,000 Å $^3$  cantered on a fibril trimer. For each compound, the search genetic algorithm was run 50 times for each receptor model using the desolvation scoring function to rank the solutions. The poses with negative docking scores were further analyzed by clustering and visual inspection.

### 3. Results and discussion

### 3.1. Preparation and spectroscopic properties of DMN-BocK

The straightforward synthesis of DMN-BocK consisted of two steps (Scheme 1) and led to a final yield of 60 %. Briefly, commercially available 4-bromo-1,8-naphthalic anhydride was functionalized with a

dimethylamino group using 3-dimethylaminopropionitrile. The fluorophore thus obtained was subsequently incorporated into the side chain of Boc-Lys-OH in refluxing 5:1 dioxane/water, in the presence of  $NaHCO_3$ .

The resulting lysine derivative DMN-BocK was stable in aqueous solution at room temperature for at least one month (Figure A.9). DMN-BocK is soluble at 2 mM in a range of organic solvents and in neutral to alkali aqueous solutions. When decreasing the solvent dielectric constant ( $\varepsilon$ ), the maximum emission wavelength ( $\lambda_{\rm em}$ ) of the dye solutions is blue-shifted and the emission increases significantly (Fig. 1 and A.10). For instance, the intensity in DCM was almost 1900 times higher than that in 100 mM HEPES.

The experimental dependence between  $\lambda_{\rm em}$  of DMN-BocK and  $\varepsilon$  of the solvent could be fitted to linearity as  $\lambda_{\rm em}=13.4\,{\rm Ln}(\varepsilon)+482.8$  (Fig. 1c). Since  $\varepsilon$  correlates with the refractive index  $(n_{\rm s})$ ,  $\lambda_{\rm em}$  of the dye did correlate linearly with the Bayliss function ( $f_{\rm B}$ ) of the refractive index  $(n_{\rm s})$  of the solvent (Eq. (4), Figure A.11) [32]:

$$f_B = \frac{n_s^2 - 1}{2n_s^2 + 1} \tag{4}$$

It should be noted that DMN-BocK emission slightly blueshifts in water upon increasing its concentration up to 65.5  $\mu M$  (Figure A.12). Such a feature suggested the formation of aggregates, as confirmed by measurements of dynamic light scattering (Figure A.13). The existence of a second fluorescence lifetime value  $(\tau_2)$  in other solvents like methanol, acetonitrile and acetone suggests that aggregates are also forming in these less polar solvents, but they could not be detected by dynamic light scattering (data not shown). Aggregation has been reported for other 1,8-naphthalimide derivatives in highly polar solvents [33]. Stock solutions of DMN-BocK in DMSO were used in all subsequent studies, for which aggregation was not observed.

Solvent-induced spectral shifts are generally interpreted in terms of the Lippert–Mataga equation (2), which describes Stokes shifts in terms of the change in the dipole moment of the fluorophore, and the dependence of the energy of the dipole on the dielectric constant and refractive index of the solvent, as shown in Eq. (3) [34]. The Lippert–Mataga plot for DMN-Bock (Fig. 1d) shows a good linear relationship between the Stokes' shift and the solvent orientation polarizability ( $\Delta f$ ) for those solvents in which no aggregates are formed (black dots). Those solvents where dye aggregation occurs, such as acetone, ethanol, methanol, acetonitrile and water, deviate notably from the linear correlation. It should be noted that Lippert-Mataga equation only considers the general solvent effect but it does not reflect specific solvent–fluorophore and fluorophore-fluorophore interactions [35].

### 3.2. DMN-BocK detects proteins in amyloid conformations

The amyloid model proteins lysozyme and insulin, and various polymorphs of the amyloid prion-forming domain of HET-s (*viz.*, HET-s PFD), were first used to assess the ability of DMN-BocK to detect amyloid structures. The commonly-used ThT dye was selected as a reference for comparison. As shown in Fig. 2, DMN-BocK could detect amyloid aggregates of lysozyme, insulin, and HET-s PFD fibers formed under acidic conditions, similar to ThT. DMN-BocK could also sense HET-s fibrils formed at neutral pH, which ThT cannot (Fig. 2a, blue).

The sensing capability of DMN-BocK was further studied for a range of unrelated amyloids (see Appendix 1). The presence of fibril-like aggregates was confirmed by transmission electron microscopy (TEM) (Figure A.14). As depicted in Fig. 3, DMN-BocK can detect amyloid fibers of amylin core sequences (wild-type, reverse and scrambled sequences), Prion Protein (vPrP), Sup35 and Ure2p, 4R tau and  $\alpha$ -synuclein. The emission intensity of ThT varies notably with the protein analyzed (e.g., high intensity for Sup35 and very low intensity for PrP and Ure2p), whereas DMN-BocK could sense the aggregates of all of the tested proteins, including vPrP and Ure2p, showcasing a wider coverage than ThT

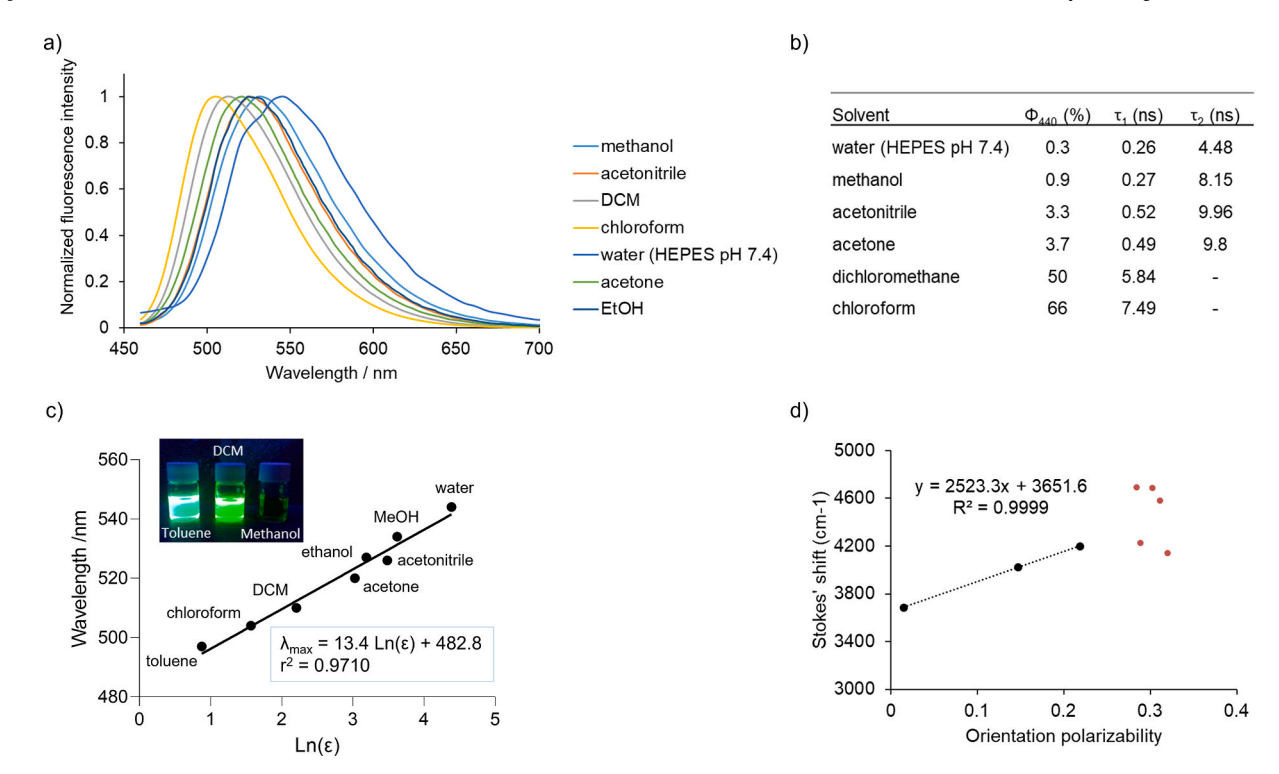


Fig. 1. a) Normalized emission spectra of DMN-BocK in different solvents. b) Relative fluorescence quantum yields (Φ) and lifetimes of DMN-BocK in different solvents. Fluorescence lifetime values  $\tau_2$  could be attributed to fluorescent aggregates of the dye. c) Dependence of  $\lambda_{em}$  of DMN-BocK with the solvent dielectric constant ( $\varepsilon$ ).  $\varepsilon$  values were taken from Ref. [31] Inset: DMN-BocK solutions in toluene, DCM, and methanol under a UV lamp. d) Lippert–Mataga plot showing Stokes' shift as a function of solvent orientation polarizability (Δf). Data corresponding to acetone, acetonitrile, ethanol, methanol and water (depicted as red dots) are not included in the linear fitting.

for detecting amyloids. Interestingly, while the  $\lambda_{em}$  of ThT does not shift significantly, the  $\lambda_{em}$  of DMN-BocK changes notably depending on the local microenvironment of the fibril-bound dye, which demonstrates distinct surface polarities (Fig. 3). Such variations of  $\lambda_{em}$  are concentration-independent. Consequently, each tested protein is distinguishable based on both the intensity and the shift of the emission of the probe. These observations suggest a broader versatility of DMN-BocK as a fluorescent probe of amyloids, compared to ThT.

# 3.3. Dielectric constants of protein binding pockets can be estimated using DMN-BocK to identify proteins

Following the above-mentioned observations and the correlation found between the solvent dielectric constant and the  $\lambda_{em}$ , we hypothesized that DMN-BocK could be used to estimate the apparent dielectric constant ( $\epsilon^{app}$ ) of the protein region it binds. Since the dielectric constant of a protein binding pocket is an intrinsic property of the protein, this measurement can potentially be exploited for protein identification and differentiation.

Using the linear function obtained above (Fig. 1c):  $\lambda_{em}=13.4\ Ln(\epsilon)+482.8$ , we interpolated the  $\epsilon^{app}$  value of the protein binding pocket of each tested protein. The calculated  $\epsilon^{app}$  value for each protein and its experimental  $\lambda_{em}$  value, is listed in Table 1.

In some cases,  $\epsilon^{app}$ , which is related to the polarity of the microenvironment within the binding pockets of the proteins, is similar for distinct amyloids. This suggests that these proteins have similar binding sites and/or macroscopic structural similarities on the fibrillar surface. This is the case for 4R tau and A $\beta$ 40 ( $\epsilon^{app}=33.9$ ), for amylin (reverse) and Ure2p ( $\epsilon^{app}=42.4$ ), and for amylin (scrambled) and Sup35 ( $\epsilon^{app}=49.2$ ).

## 3.4. DMN-BocK can distinguish protein polymorphs through the maximum emission wavelength

To investigate the capability of DMN-BocK to differentiate the structures of fibrillar polymorphs of a protein, we selected Ure2p yeast prion fibers, because their structures depend on the formation temperature [36]. When increasing the incubation temperature from 20 to 50 °C, Ure2p flexible regions within the fibrils reorganize gradually into more rigid  $\beta$ -sheet structures, and a stronger emission of the probe is observed with a concomitant blue shift from 544 to 533 nm (Figure A.15). As depicted in Fig. 4, the calculated  $\epsilon^{app}$  values were found to correlate with reported data on (i) the absorbance at 1629 cm<sup>-1</sup> (amide I region), which relates with the  $\beta$ -sheet content, and (ii) the proteinase K-digested fraction, which relates to the amyloid stability of the respective Ure2p polymorphs [36].

Common amyloid probes like Congo Red (CR) or ThT can detect temperature-driven conformational changes exclusively through a concentration-dependent magnitude, viz. the absorbance (CR) and the emission intensity (ThT) [37]. DMN-BocK allows to differentiate polymorphs of a given protein in a non-concentration-dependent parameter as  $\lambda_{\rm em}$ . ThT and CR spectroscopic data correlate with the calculated  $\epsilon^{\rm app}$  using DMN-BocK (Figure A.16).

# 3.5. Binding stoichiometry and affinity of DMN-BocK to amyloid fibers of $A\beta 40$

The A $\beta$ 40 peptide was selected to gain further insight into the interaction of our solvatochromic probe with amyloid proteins. A $\beta$ 40 is associated with Alzheimer's disease progression. In the presence of preformed A $\beta$ 40 fibers (ThT positive), DMN-BocK fluorescence increases and undergoes a blue shift of 17 nm (Figure A.17). Deconvolution of the A $\beta$ -bound DMN-BocK emission spectrum into three peaks (I, II and III) indicates that the area of peak I increases from 2.6 to 10.4 % in the

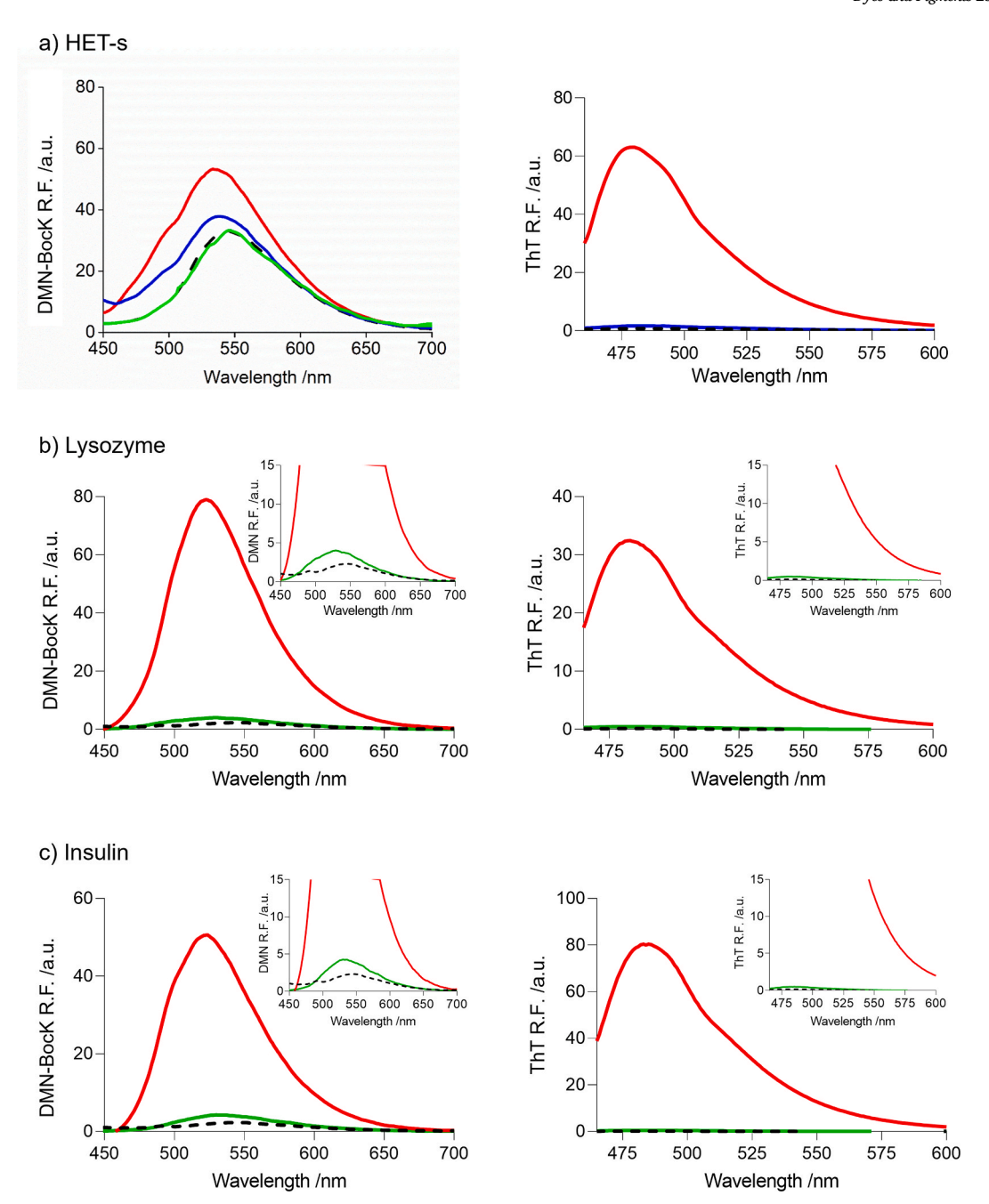


Fig. 2. Emission spectra of DMN-Bock (left) and ThT (right) of (a) HET-s PFD (green: monomers; red: pH 2 fibers; blue: pH 7 fibrils); b) lysozyme (red: fibers; green: native protein), and c) insulin (red: fibers; green: native protein). The dotted black spectra correspond to the free fluorescent probe.

presence of A $\beta$  fibrils, while peaks II and III do not change significantly (Fig. 5a). Thus, peak I may be regarded as the "amyloid band" because it characterizes the presence of  $\beta$ -sheets.

Considering the emission data of free and A $\beta$ -bound DMN-BocK (Figure A.18), the dissociation constant ( $K_d$ ), the maximum concentration of A $\beta$ -bound dye ( $B_{max}$ ), and the stoichiometry of the A $\beta$ -dye complex (n) could be determined using the typical one-site binding equation (saturation binding curve, Eq. (5)):

$$y = \frac{B_{max} \cdot x}{K \cdot L \cdot Y} \tag{5}$$

where y is the concentration of DMN-BocK bound to Aβ40, and x is the dye concentration.

The resulting Scatchard plot (Fig. 5b) yielded a  $K_d$  value of 2.1  $\mu$ M and a  $B_{max}$  of 2.0  $\mu$ M. The Scatchard analysis also indicated an A $\beta$ 40-to-

DMN-BocK binding ratio of 5, which was corroborated by molecular docking (Section 3.6, Fig. 5c).

### 3.6. DMN-BocK and ThT compete for binding $A\beta 40$

When DMN-BocK is gradually added to a preincubated solution of ThT and A $\beta$ 40 fibers, the characteristic emission of ThT-bound A $\beta$ 40 decreases while a partially overlapping band, attributable to A $\beta$ -bound DMN-BocK emerges around 525–530 nm (Fig. 6). These changes are likely due to the displacement of ThT by DMN-BocK, which suggests a common binding site for both probes [38,39].

Docking calculations were carried out with DMN-BocK and ThT to determine their possible binding site(s); 20 different conformers obtained from the A $\beta$ 40 fibril NMR ensemble (PDB id 2M4J) were used. For DMN-BocK, docking poses with favorable docking scores were identified

G. Vázquez et al. Dyes and Pigments 231 (2024) 112348

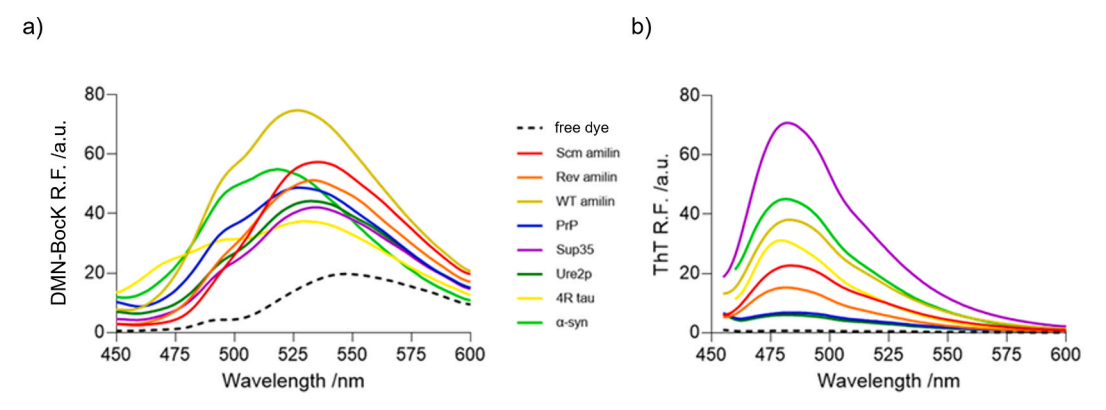


Fig. 3. Emission spectra of DMN-BocK (25  $\mu$ M; left) and ThT (25  $\mu$ M; right) after 5-min incubation at room temperature with fibers of different proteins. [Protein] = 20  $\mu$ M; PBS pH 7.4.

**Table 1** Calculated apparent dielectric constant values ( $\epsilon^{app}$ ) of the binding microenvironment of DMN-BocK in different amyloid fibers in PBS, pH 7.4.

Protein	$\lambda_{\rm em}$ (nm)	$\varepsilon^{\mathrm{app}}$
4R tau	530	33.9
α-syn	518	13.8
Lysozyme	523	20.1
Insulin	524	21.6
Amylin (wild type)	527	27.1
Amylin (reverse)	533	42.4
Amylin (scrambled)	535	49.2
PrP	526	25.1
HETs-PFD (pH 2 fibers)	534	45.6
HETs-PFD (pH 7 fibrils)	539	66.3
Αβ40	530	33.9
Ure2p	533	42.4
Sup35	535	49.2

in only four cases, with energy values ranging from -10.3 to -4.0 kJ mol $^{-1}$ . For ThT, the number of conformations leading to binding poses with associated negative docking scores was ten out of twenty, with energy values ranging from -27.1 to -4.4 kJ mol $^{-1}$ . These data indicate that ThT can bind to a more diverse set of A $\beta$ 40 conformations and, in some cases, with a relatively high affinity. These observations are consistent with the widespread use of this molecule as a fluorescent probe to assess A $\beta$ 40 aggregation. Interestingly, the most observed binding site yielding favorable docking poses for both dyes was the narrow cleft delineated between the sidechains of residues Phe4 and

His6 on each side, and the backbone of residue Arg5 at the bottom. Specifically, three out of four suitable binding poses for DMN-BocK and seven out of ten poses for ThT were identified in this cleft. Furthermore, the best-scored pose for each compound in the 4-5-6 cleft displayed similar  $\pi$ -stacking interactions with the sidechain of Phe4 (Fig. 7), with qualitatively comparable binding scores of -9.9 and -13.6 kJ mol $^{-1}$  for DMN-BocK and ThT, respectively. A  $\beta$ -stacking interaction with an available aromatic amino acid residue was also identified in previous studies of the interaction between ThT and A $\beta$ 42 [39].

While the Phe4-Arg5-His6 crevice was the best-scored binding site for DMN-BocK and the most common one for ThT across the 20 NMR models studied, ThT was predicted to favorably bind with either better or similar affinity to two additional binding sites (Figure A.19). Specifically, the lowest binding energy ( $-27.1 \text{ kJ mol}^{-1}$ ) was found for ThT occupying the pocket delineated by residues Phe20, Lys28, and Ile31 (NMR conformer 12 in the 2M4J structure, Figure A.19a). In contrast, the tricyclic moiety of DMN-BocK is too sterically hindered to adopt a similar binding mode. An additional binding site was identified for ThT at the crevice delineated by residues His6-Ser8-Tyr10 (Figure A.19b).

In summary, the docking results suggest that competitive binding between DMN-BocK and ThT is taking place at the 4-5-6 cleft, although the smaller ThT molecule is also likely to occupy other hydrophobic pockets within the fibril, thus saturating all accessible binding sites within the A $\beta$ 40 aggregates. Moreover, the importance of  $\pi$ -stacking interactions with the sidechain of Phe4 in the interaction with A $\beta$ 40, and hence, in the recognition of amyloid conformation, implies that other 4-DMN-functionalized amino acids such as the alanine one described by Loving et al. are potentially able to sense amyloid aggregation as well.

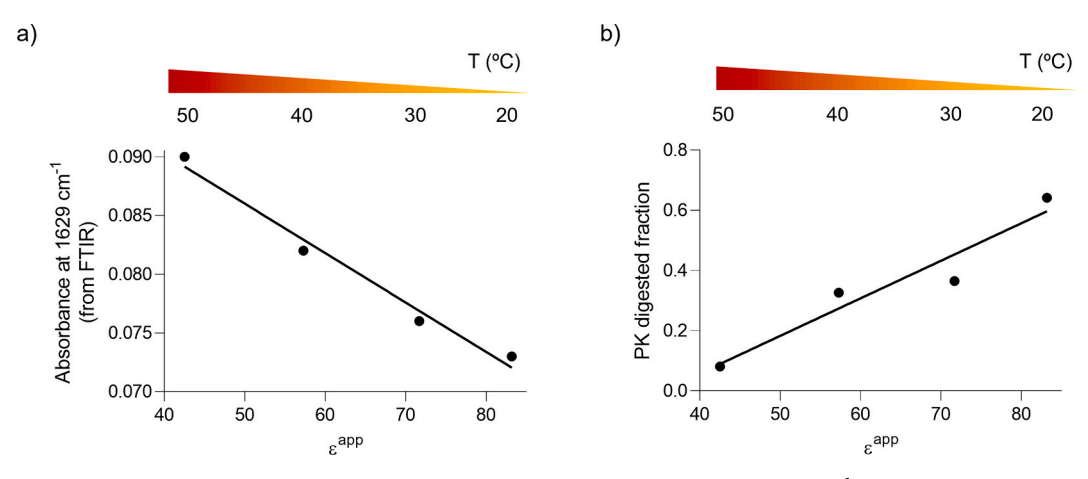


Fig. 4. Correlation between the calculated  $\epsilon^{app}$  (DMN-BocK) values and a) the FTIR absorbance band at 1629 cm $^{-1}$ , and b) the proteinase K-digested fraction of Ure2p fibrils preincubated at 20, 30, 40 and 50 °C. FTIR and PK-resistant fraction data have been extracted from Ref. [36] [Ure2p] = 35  $\mu$ M, [DMN-BocK] = 10  $\mu$ M, in NB.

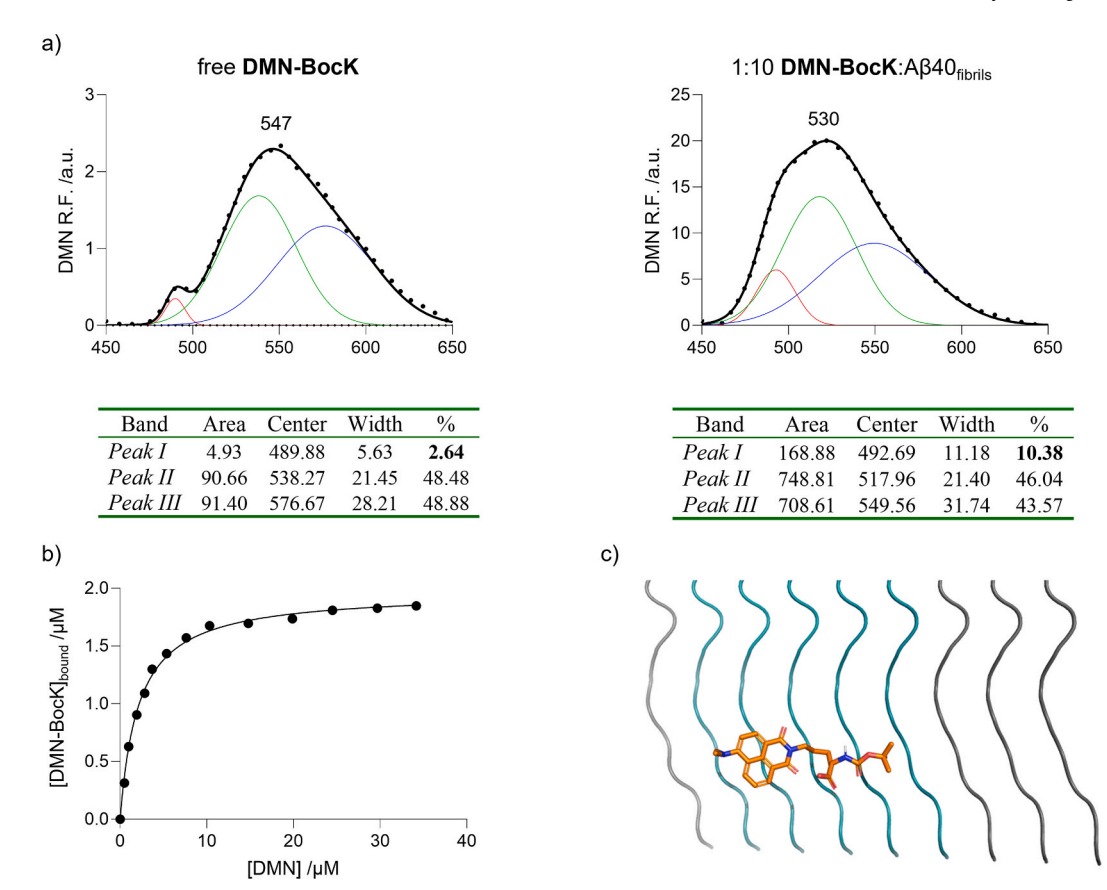
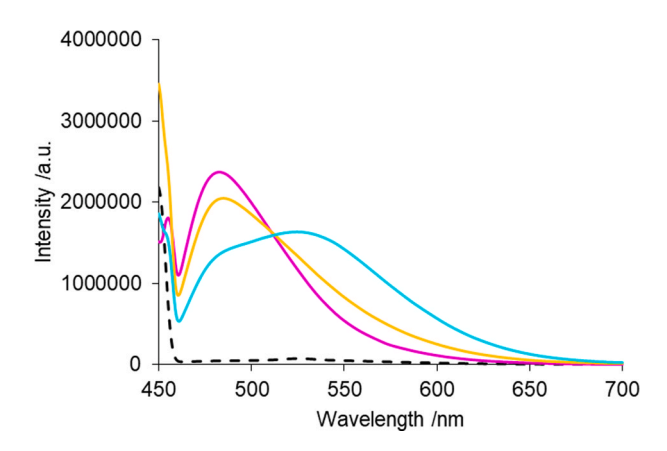


Fig. 5. a) Deconvolution analysis of the emission band of DMN-BocK. Left: free DMN-BocK (5  $\mu$ M); Right: 5  $\mu$ M DMN-BocK incubated with Aβ40 fibers (50  $\mu$ M) in 100 mM HEPES, pH 7.4,  $\lambda_{ex}$  420 nm; b) Scatchard plot of DMN-BocK binding to Aβ40; c) Proposed binding by Scatchard analysis: 1 DMN-BocK for 5 Aβ40 peptides (in green). The presence of fibers was confirmed by ThT fluorescence.



**Fig. 6.** Emission spectra upon addition of 0 eq (pink), 0.5 eq (yellow), and 2.5 eq (blue) of DMN-BocK to ThT-bound fibers of Aβ40. The dashed black line corresponds to free DMN-BocK. [ThT] = 5 μM, [Aβ40] = 10 μM, 100 mM HEPES pH 7.4.  $\lambda_{\rm ex} = 445$  nm. The samples were incubated at 37 °C for 15 min after each addition.

# 3.7. DMN-BocK is suitable for monitoring the aggregation of $A\beta40$ both in vitro and in cellulo by fluorescence

 $A\beta40$  aggregation was monitored concomitantly by (i) absorbance at 360 nm (scattering), (ii) fluorescence at 490 nm (ThT), and (iii) fluorescence at 530 nm (DMN-BocK). Fig. 8a shows that the aggregation follows a characteristic two-step autocatalytic sigmoidal curve, which results from two sequential processes: nucleation and elongation (Scheme A.1). The curves were rather similar for the three detection

methods, and their fitting provided rather similar nucleation times ( $t_0$ ) (see fitting details in Appendix A and Table A.1). These results confirm that DMN-BocK may be used as an alternative to ThT for monitoring *in vitro* protein aggregation, which might include ThT-silent amyloids.

ThT cannot be used *in cellulo* (e.g. bacteria) because of its poor permeability through cell membranes; this fact has been attributed to the low lipophilicity of the dye [40]. The lipophilicity can be expressed numerically by the lipophilicity partition coefficient (P) between octan-1-ol and water; the higher P is, the less lipophilic is the substance. The calculated log P value of ThT is 1.15, which is lower that the log P value of DMN-BocK (3.55). Therefore, the new probe is expected to show a stronger preference for hydrophobic environments than ThT.

The potential of DMN-BocK for crossing cell membranes was confirmed using Gram-negative bacteria ( $\it E.~coli$ ) overexpressing A $\beta$ 40. Our probe was compared with ThS as a reference for monitoring amyloid aggregation in cellulo. The kinetic curves shown in Fig. 8b demonstrate that DMN-BocK can also detect and monitor protein aggregation within cells. The fitting of the aggregation curves using ThS and DMN-BocK produced rather similar kinetic parameters (Table S2), thus showing that DMN-BocK can replace the use of ThS.

Confocal microscopy confirmed that DMN-BocK can penetrate bacterial cells satisfactorily, enabling the staining of amyloid aggregates within the cells. In the micrographs (Fig. 8c), amyloid inclusion bodies (white arrows) can be observed as refractile structures inside *E. coli* cells overexpressing A $\beta$ 42, A $\beta$ 40 and tau. The fluorescence of DMN-BocK is more intense in the poles of the cells coinciding with higher-density regions.

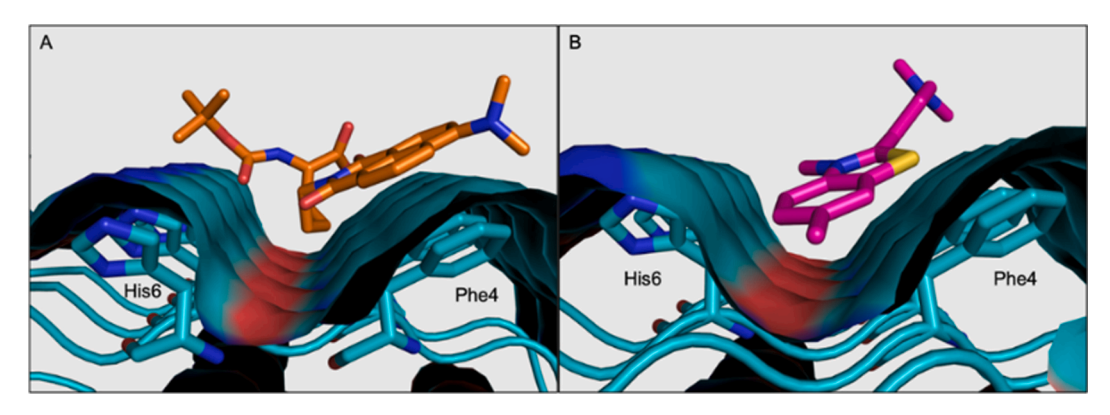


Fig. 7. Binding mode of a) DMN-BocK and b) ThT at the Phe4-Arg5-His6 crevice. For clarity, some Aβ40 monomers are not displayed.

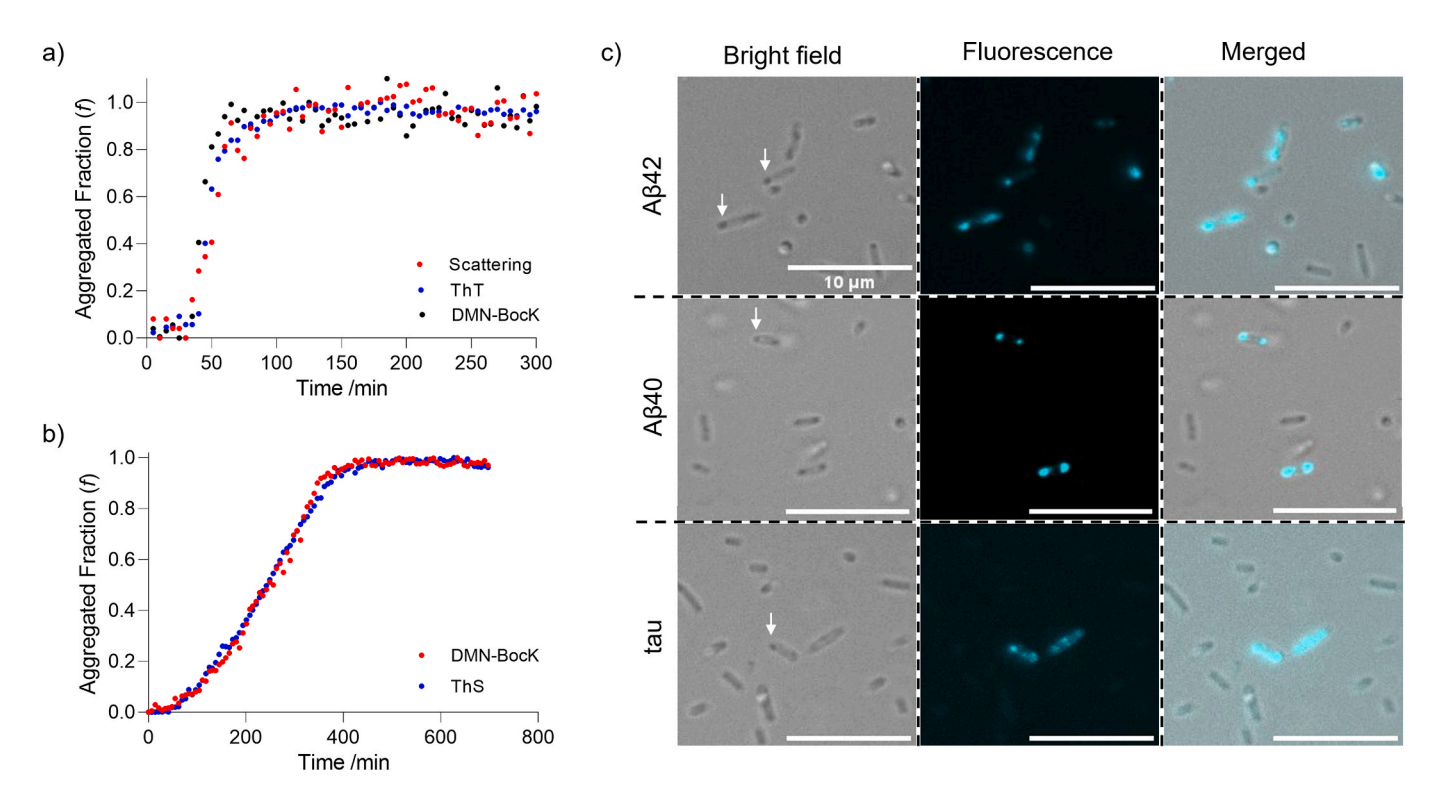


Fig. 8. a) *In vitro* aggregation kinetics of Aβ40 monitored by light scattering, ThT emission, and DMN-BocK emission; b) Aggregation kinetics of Aβ40 monitored by emission of DMN-BocK and ThS in bacteria; c) Confocal micrographs of DMN-BocK-stained *E. coli* cells overexpressing Aβ42, Aβ40 and tau.

#### 4. Conclusions

A versatile fluorescent probe, sensitive to microenvironments has been obtained in good yield in two steps. It consists of a lysine residue with a 4-DMN moiety connected to its side chain. Similarly to other DMN derivatives, the emission of DMN-BocK is sensitive to solvent polarity. We demonstrated that DMN-BocK can sense small polar variations within the (usually hydrophobic) binding pockets of amyloids. In contrast to probes of choice in amyloid research, DMN-BocK can differentiate amyloid structures of disease-related proteins, including polymorphs, thanks to an extrapolation of the dielectric constant ( $\epsilon^{app}$ ) of their binding pocket. *In vitro* studies along with molecular docking calculations suggest that DMN-BocK binds A $\beta$ 40 1-to-5 and competes with ThT binding at the 4-5-6 cleft. Furthermore, this new sensing molecule can monitor the aggregation process of A $\beta$ 40 both *in vitro* and *in cellulo* (Gram-negative bacteria), which shows that, unlike ThT, DMN-BocK can penetrate membranes and probe fibril formation inside cells.

By yielding the  $\epsilon^{app}$  of the probe-protein binding pocket, DMN-BocK can help improve molecular dynamics simulations using implicit

solvation, enabling a more accurate representation of the binding site microenvironment than the commonly used value of  $\epsilon^{app}=1$  [41].

All in all, DMN-BocK represents an important contribution to the current fluorogenic toolbox of sensors. This DMN-functionalized amino acid may be used to design (biocompatible) probes for early detection and monitoring of disease-related protein aggregation and other biological processes [1]. Early diagnosis can be key for successful therapy, particularly for incurable neurodegenerative pathologies such as Alzheimer's and Parkinson's [42].

#### CRediT authorship contribution statement

Guillem Vázquez: Writing – original draft, Methodology, Investigation, Formal analysis, Data curation. Alba Espargaró: Writing – original draft, Visualization, Validation, Methodology, Investigation, Formal analysis, Data curation. Ana B. Caballero: Writing – review & editing, Writing – original draft, Visualization, Validation, Supervision, Methodology, Investigation, Formal analysis, Data curation, Conceptualization. Ania Di Pede-Mattatelli: Investigation, Formal analysis, Data

curation. **M. Antònia Busquets:** Investigation. **Daria Nawrot:** Investigation. **Raimon Sabaté:** Writing – review & editing, Writing – original draft, Visualization, Methodology, Investigation, Formal analysis, Data curation, Conceptualization. **Ernesto Nicolás:** Supervision, Methodology, Formal analysis. **Jordi Juárez-Jiménez:** Writing – original draft, Methodology, Investigation, Formal analysis, Data curation, Conceptualization. **Patrick Gamez:** Writing – review & editing, Writing – original draft, Supervision, Funding acquisition.

### Declaration of competing interest

The authors declare that they have no known competing financial interests or personal relationships that could have appeared to influence the work reported in this paper.

## Data availability

Data will be made available on request.

#### Acknowledgment

We thank Dr. P. P Güixens-Gallardo and Dr. B. Limburg for their respective assistance with quantum yield and time-correlated single photon counting (TCSPC) measurements. Financial support from the Spanish Ministerio de Ciencia, Innovación e Universidades (Projects PID2020-115537RB-I00, PID2021-127863OB-I00, PID2020-115683GA-I00, CEX2021-001202-M, MCIU/AEI/10.13039/501100011033 and European Union NextGenerationEU/PRTR) is acknowledged. P.G. thanks the Institució Catalana de Recerca i Estudis Avançats (ICREA). Generalitat de Catalunya is acknowledged for supporting the 2021SGR00668 and 2021SGR00671 groups.

### Appendix A. Supplementary data

Supplementary data to this article can be found online at https://doi.org/10.1016/j.dyepig.2024.112348.

#### References

- Liu L, Huang Y, Zhou Y, Zhao Y, Qi J, Zhang X, et al. Fluorogenic toolbox for visualizing protein aggregation: from designing principles to biological application. TrAC, Trends Anal Chem 2022;157:116764.
- [2] Zhu C, Kwok RTK, Lam JWY, Tang BZ. Aggregation-induced emission: a trailblazing journey to the field of biomedicine. ACS Appl Bio Mater 2018;1(6): 1768–86.
- [3] Loving GS, Sainlos M, Imperiali B. Monitoring protein interactions and dynamics with solvatochromic fluorophores. Trends Biotechnol 2010;28(2):73–83.
- [4] Qin X, Yang X, Du L, Li M. Polarity-based fluorescence probes: properties and applications. RSC Med Chem 2021;12(11):1826–38.
- [5] Espinar-Barranco L, Paredes JM, Orte A, Crovetto L, Garcia-Fernandez E. A solvatofluorochromic dye as a fluorescent lifetime-based probe of β-amyloid aggregation. Dyes Pigments 2022;202:110274.
- [6] Yang J, Zeng F, Ge Y, Peng K, Li X, Li Y, et al. Development of near-infrared fluorescent probes for use in Alzheimer's disease diagnosis. Bioconjugate Chem 2020;31(1):2–15.
- [7] Cao KJ, Elbel KM, Cifelli JL, Cirera J, Sigurdson CJ, Paesani F, et al. Solvation-guided design of fluorescent probes for discrimination of amyloids. Sci Rep 2018;8 (1):6950
- [8] Yates EV, Meisl G, Knowles TP, Dobson CM. An environmentally sensitive fluorescent dye as a multidimensional probe of amyloid formation. J Phys Chem B 2016;120(9):2087–94.
- [9] Cao K, Farahi M, Dakanali M, Chang WM, Sigurdson CJ, Theodorakis EA, et al. Aminonaphthalene 2-cyanoacrylate (ANCA) probes fluorescently discriminate between amyloid-beta and prion plaques in brain. J Am Chem Soc 2012;134(42): 17338–41.
- [10] Loving G, Imperiali B. A versatile amino acid analogue of the solvatochromic fluorophore 4-N,N-dimethylamino-1,8-naphthalimide: a powerful tool for the study of dynamic protein interactions. J Am Chem Soc 2008;130(41):13630-8.
- [11] Casey GR, Zhou X, Lesiak L, Xu B, Fang Y, Becker DF, et al. An evolutionary strategy for identification of higher order, green fluorescent host-guest pairs compatible with living systems. Chemistry 2020;26(70):16721–6.
- [12] Berque-Bestel I, Soulier J-L, Giner M, Rivail L, Langlois M, Sicsic S. Synthesis and characterization of the first fluorescent antagonists for human 5-HT4 receptors. J Med Chem 2003;46(13):2606–20.

- [13] Fueyo-González F, Fernández-Gutiérrez M, García-Puentes D, Orte A, González-Vera JA, Herranz R. Naphthalimide-based macrophage nucleus imaging probes. Eur J Med Chem 2020;200:112407.
- [14] Betancourt F, Valente A, Yan H. 1,8-Naphthalimide derivatives as probes for protein surface hydrophobicity. J Photochem Photobiol Chem 2021;418:113386.
- [15] Ke Y, Cao J, Gong J, Fu N. A near-infrared naphthalimide fluorescent probe for targeting the lysosomes of liver cancer cells and specifically selecting HSA. Sensor Actuator B Chem 2022;352:131015.
- [16] McLean AM, Socher E, Varnavski O, Clark TB, Imperiali B, Goodson 3rd T. Two-photon fluorescence spectroscopy and imaging of 4-dimethylaminonaphthalimide peptide and protein conjugates. J Phys Chem B 2013;117(50):15935–42.
- [17] Fueyo-Gonzalez F, Gonzalez-Vera JA, Alkorta I, Infantes L, Jimeno ML, Aranda P, et al. Environment-sensitive probes for illuminating amyloid aggregation in vitro and in zebrafish. ACS Sens 2020;5(9):2792–9.
- [18] Ruiz-Arias Á, Jurado R, Fueyo-González F, Herranz R, Gálvez N, González-Vera JA, et al. A FRET pair for quantitative and superresolution imaging of amyloid fibril formation. Sensor Actuator B Chem 2022;350:130882.
- [19] Aliyan A, Cook NP, Martí AA. Interrogating amyloid aggregates using fluorescent probes. Chem Rev 2019;119(23):11819–56.
- [20] Graziotto ME, Adair LD, Kaur A, Verite P, Ball SR, Sunde M, et al. Versatile naphthalimide tetrazines for fluorogenic bioorthogonal labelling. RSC Chem Biol 2021;2(5):1491-8.
- [21] Zhang Z, Yuan Q, Li M, Bao B, Tang Y. A ratiometric fluorescent conjugated oligomer for amyloid beta recognition, aggregation inhibition, and detoxification. Small 2021;17(52):e2104581.
- [22] Sasaki S, Drummen GPC, Konishi G-i. Recent advances in twisted intramolecular charge transfer (TICT) fluorescence and related phenomena in materials chemistry. J Mater Chem C 2016;4(14):2731–43.
- [23] Xue C, Lin TY, Chang D, Guo Z. Thioflavin T as an amyloid dye: fibril quantification, optimal concentration and effect on aggregation. R Soc Open Sci 2017;4(1):160696.
- [24] Maskevich AA, Stsiapura VI, Kuzmitsky VA, Kuznetsova IM, Povarova OI, Uversky VN, et al. Spectral properties of thioflavin T in solvents with different dielectric properties and in a fibril-incorporated form. J Proteome Res 2007;6(4): 1392–401.
- [25] Sabate R, Rodriguez-Santiago L, Sodupe M, Saupe SJ, Ventura S. Thioflavin-T excimer formation upon interaction with amyloid fibers. Chem Commun 2013;49 (51):5745–7.
- [26] Ren H, Fingerhut BP, Mukamel S. Time resolved photoelectron spectroscopy of thioflavin T photoisomerization: a simulation study. J Phys Chem A 2013;117(29): 6096–104.
- [27] Stsiapura VI, Maskevich AA, Kuzmitsky VA, Turoverov KK, Kuznetsova IM. Computational study of thioflavin T torsional relaxation in the excited state. J Phys Chem 2007;111(22):4829–35.
- [28] Ruiz-Carmona S, Alvarez-Garcia D, Foloppe N, Garmendia-Doval AB, Juhos S, Schmidtke P, et al. rDock: a fast, versatile and open source program for docking ligands to proteins and nucleic acids. PLoS Comput Biol 2014;10(4):e1003571.
- [29] Lu JX, Qiang W, Yau WM, Schwieters CD, Meredith SC, Tycko R. Molecular structure of beta-amyloid fibrils in Alzheimer's disease brain tissue. Cell 2013;154 (6):1257–68.
- [30] Olsson MHM, Søndergaard CR, Rostkowski M, Jensen JH. PROPKA3: consistent treatment of internal and surface residues in empirical pKa predictions. J Chem Theor Comput 2011;7(2):525–37.
- [31] Haynes WML DR, Bruno TJ, editors. CRC handbook of chemistry and physics. 95th edition. CRC Press. Taylor & Francis Group; 2014.
- [32] Sabaté R, Estelrich J. Determination of micellar microenvironment of pinacyanol by visible spectroscopy. J Phys Chem B 2003;107(17):4137–42.
- [33] Cho DW, Cho DW. Excimer and exciplex emissions of 1,8-naphthalimides caused by aggregation in extremely polar or nonpolar solvents. New J Chem 2014;38(6): 2233–6.
- [34] Mataga N, Kaifu Y, Koizumi M. Solvent effects upon fluorescence spectra and the dipolemoments of excited molecules. Bull Chem Soc Jpn 1956;29(4):465–70.
- [35] Solvent and environmental effects. In: Lakowicz JR, editor. Principles of fluorescence spectroscopy. Boston, MA: Springer US; 2006. p. 205–35.
- [36] Sabate R, Villar-Pique A, Espargaro A, Ventura S. Temperature dependence of the aggregation kinetics of Sup35 and Ure2p yeast prions. Biomacromolecules 2012;13 (2):474–83.
- [37] Espargaro A, Llabres S, Saupe SJ, Curutchet C, Luque FJ, Sabate R. On the binding of Congo red to amyloid fibrils. Angew Chem 2020;59(21):8104–7.
- [38] Krebs MR, Bromley EH, Donald AM. The binding of thioflavin-T to amyloid fibrils: localisation and implications. J Struct Biol 2005;149(1):30-7.
- [39] Rodriguez-Rodriguez C, Rimola A, Rodriguez-Santiago L, Ugliengo P, Alvarez-Larena A, Gutierrez-de-Teran H, et al. Crystal structure of thioflavin-T and its binding to amyloid fibrils: insights at the molecular level. Chem Commun 2010;46 (7):1156–8.
- [40] Darghal N, Garnier-Suillerot A, Salerno M. Mechanism of thioflavin T accumulation inside cells overexpressing P-glycoprotein or multidrug resistance-associated protein: role of lipophilicity and positive charge. Biochem Biophys Res Commun 2006;343(2):623–9.
- [41] Li L, Li C, Zhang Z, Alexov E. On the dielectric "constant" of proteins: smooth dielectric function for macromolecular modeling and its implementation in DelPhi. J Chem Theor Comput 2013;9(4):2126–36.
- [42] Porsteinsson AP, Isaacson RS, Knox S, Sabbagh MN, Rubino I. Diagnosis of early Alzheimer's disease: clinical practice in 2021. J Prev Alzheimers Dis 2021;8(3): 371–86.